TiNi-based films for elastocaloric microcooling— Fatigue life and device performance

H. Ossmer, C. Chluba, S. Kauffmann-Weiss, E. Quandt, and M. Kohl

Citation: APL Mater. **4**, 064102 (2016); doi: 10.1063/1.4948271

View online: http://dx.doi.org/10.1063/1.4948271

View Table of Contents: http://scitation.aip.org/content/aip/journal/aplmater/4/6?ver=pdfcov

Published by the AIP Publishing

TiNi-based films for elastocaloric microcooling—Fatigue life and device performance

H. Ossmer,[1] C. Chluba,[2] S. Kauffmann-Weiss,[3] E. Quandt,[2] and M. Kohl[1]
[1]*Institute of Microstructure Technology, Karlsruhe Institute of Technology, P.O. Box 3640, 76021 Karlsruhe, Germany*
[2]*Institute for Materials Science, Faculty of Engineering, University of Kiel, 24143 Kiel, Germany*
[3]*Institute for Technical Physics, Karlsruhe Institute of Technology, P.O. Box 3640, 76021 Karlsruhe, Germany*

(Received 26 February 2016; accepted 14 April 2016; published online 28 April 2016)

The global trend of miniaturization and concomitant increase of functionality in microelectronics, microoptics, and various other fields in microtechnology leads to an emerging demand for temperature control at small scales. In this realm, elastocaloric cooling is an interesting alternative to thermoelectrics due to the large latent heat and good down-scaling behavior. Here, we investigate the elastocaloric effect due to a stress-induced phase transformation in binary TiNi and quaternary TiNiCuCo films of 20 μm thickness produced by DC magnetron sputtering. The mesoscale mechanical and thermal performance, as well as the fatigue behavior are studied by uniaxial tensile tests combined with infrared thermography and digital image correlation measurements. Binary films exhibit strong features of fatigue, involving a transition from Lüders-like to homogeneous transformation behavior within three superelastic cycles. Quaternary films, in contrast, show stable Lüders-like transformation without any signs of degradation. The elastocaloric temperature change under adiabatic conditions is −15 K and −12 K for TiNi and TiNiCuCo films, respectively. First-of-its-kind heat pump demonstrators are developed that make use of out-of-plane deflection of film bridges. Owing to their large surface-to-volume ratio, the demonstrators reveal rapid heat transfer. The TiNiCuCo-based devices, for instance, generate a temperature difference of 3.5 K within 13 s. The coefficients of performance of the demonstrators are about 3. [http://dx.doi.org/10.1063/1.4948271]

Solid-state cooling based on caloric effects[1–6] has attracted large interest in recent years aiming at alternative solutions to environmentally harmful vapor compression and energy inefficient thermoelectrics.[7] Elastocaloric cooling on the basis of shape memory alloys (SMA) relies on a stress-induced phase transformation between a high temperature austenite (A) and a low temperature martensite (M) phase.[8] The latent heat associated with this diffusion-less first-order phase transformation is material-dependent, typically higher than for magnetocaloric and electrocaloric materials and may exceed 30 J/g in the case of TiNi.[9–11]

The development of elastocaloric cooling devices is just at the beginning.[12–16] Recently, first macroscale elastocaloric cooling demonstrators have been reported, reaching temperature differences between heat source and sink of 1.5 and 7 K for compressive and tensile loading of TiNi-based SMA, respectively.[17,18]

Due to favorable scaling behavior, elastocaloric cooling becomes highly attractive also for microcooling, which gains importance, e.g., in microelectronics and lab-on-chip systems.[19,20] Thin SMA films and foils are predestined for miniature applications because of their large surface-to-volume ratio, which allows for fast heat transfer.[21] Further crucial material parameters in terms of practical applications are the elastocaloric effect size, as well as functional and structural fatigue.

In this work, we compare two sputtered film materials regarding their effect size and fatigue behavior. The investigated materials are standard binary TiNi films, as well as newly developed

TiNiCu-based films that exhibit extremely high cyclic stability.[22] After presenting the material characteristics, the design, fabrication, and performance of first-of-its-kind miniature-scale demonstrators are discussed.[23]

Freestanding film samples with a thickness of 20 μm are produced by dc magnetron sputtering, followed by rapid thermal annealing. The procedure is described in Refs. 24 and 25. Sample width and length are 1.75 mm and 15 mm, respectively. Film compositions are determined by energy dispersive X-ray analysis (EDX) to be $Ti_{49.6}Ni_{50.4}$ for the binary films and $Ti_{55}Ni_{29.6}Cu_{12.6}Co_{2.8}$ for the quaternary films. In the latter case, Co is added in order to shift the austenite finish temperature A_f below ambient temperature. Phase transformation temperatures and latent heats are investigated by differential scanning calorimetry. The TiNi samples show a two-step transformation with a total latent heat of 18.9 J/g. The TiNiCuCo samples show a one-step transformation, which is considerably sharper showing a lower latent heat of 13.7 J/g.[25] The austenite finish temperatures are 20 and 14 °C, respectively, confirming that both samples are superelastic at room temperature.

In previous publications, it was shown that the cyclic stability of the TiNiCuCo films is outstanding,[22,25,26] whereas TiNi films suffer from fatigue.[26,21] In order to investigate the stress-induced phase transformation, uniaxial tensile tests are performed for both samples. During the experiment, the temperature evolution of the sample is monitored by an infrared (IR) camera, while the local strain distribution is evaluated by digital image correlation (DIC) for a small test area of 2×3 mm^2. The results of a cyclic test at a strain rate of 0.02 s^{-1} are shown in Figs. 1(a) and 1(b). The stress-strain characteristic of the binary sample exhibits a strong fatigue behavior within the first load cycles: The superelastic plateaus become steeper, the area enclosed by the curve decreases, and a considerable amount of plastic deformation is accumulated. After 20 cycles, the curve adopts a cigar-like shape and accumulates a remanent strain of 1.75%. In subsequent cycles, the mechanical behavior stabilizes. The insets of Fig. 1(a) show that sharp Lüders-like strain bands

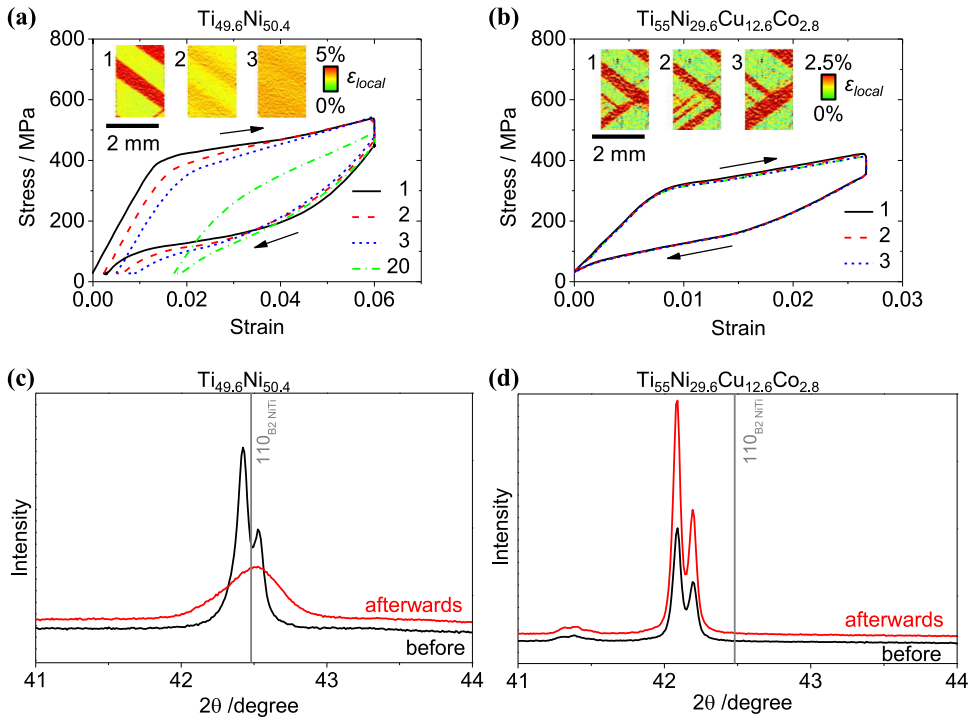

FIG. 1. Cyclic tensile experiments on superelastic film samples: stress-strain characteristics of (a) TiNi and (b) TiNiCuCo sample obtained from cyclic tensile tests at a strain rate of 0.02 s^{-1}. Ambient temperature was 24 °C for TiNi and 22 °C for TiNiCuCo sample. The cycle numbers are indicated. The insets show the local strain distribution including Lüders-like strain bands in a test area of 2×3 mm^3 during the loading stress plateau for the first, second, and third cycle. X-ray diffraction measurements are performed before and after mechanical cycling for (c) TiNi and (d) TiNiCuCo sample. A literature value for the 110 B2 peak of TiNi is included for orientation.

are observed in the first load cycle. During the following cycles, these bands become broader and eventually vanish completely.[25] The quaternary sample (Fig. 1(b)), in contrast, does not exhibit this kind of fatigue behavior. The stress-strain trajectories of different cycles coincide and sharp strain bands are consistently observed. A previous in-depth study with long-term cycling has revealed that the mechanical behavior of the newly developed TiNiCu(Co) material is actually stable for more than 10^7 cycles.[22]

The pronounced remanent strain and the changes in local deformation behavior, in particular, the disappearance of strain bands, indicate changes in microstructure due to fatigue in the binary material. In order to further investigate these changes, X-ray diffraction (XRD) measurements are conducted for both materials before and after mechanical cycling. These measurements are carried out on a Bruker D8 diffractometer in Bragg-Brentano geometry at room temperature in a two-circle setup using Cu-K_a radiation. The measurement range is between 20 and 120° and the test area is 10×5 mm^2. The results are depicted in Figs. 1(c) and 1(d). The binary TiNi samples show reflections in the XRD diagram, corresponding to the B2 austenite phase, which is consistent with the DSC results (A_f = 20 °C). The splitting of the reflection originates from $K_{\alpha1}$ and $K_{\alpha2}$ splitting of the K_α doublet. A Rietveld analysis (with the Bruker Software Topas) yields a lattice parameter of a_{B2} = 0.3012 nm with large grains and nearly strain free ($\varepsilon_0 \sim 0$). After the tensile test procedure, however, broad reflections are observed, indicating that an inhomogeneous distribution of stress states is present within the material after mechanical cycling. The Rietveld analysis reveals a_{B2} = 0.3008 nm with a small crystallite size (d = 32 nm) and a large mean microstrain value of ε_0 = 0.1652. The microstrain represents displacements of atoms from their ideal positions caused by introduction and multiplication of lattice defects, e.g., dislocations, twins, stacking faults, and similar defects. In binary TiNi, these processes are irreversible and result in the observed plastic deformation in the stress-strain curves and the peak broadening in XRD. In case of the quaternary TiNiCuCo sample, the XRD spectrum is evidently not affected by mechanical cycling. The split reflections are associated with the B2 austenite showing no broadening before and after tensile testing. Besides, the position in 2θ is shifted to lower angles with respect to the B2 peak of binary TiNi. The lattice parameter is a_{B2} = 0.3035 nm. The Rietveld analysis shows that both states are nearly strain free ($\varepsilon_0 \sim 0$). This result is in line with recent XRD and TEM measurements on Ti-rich TiNiCu films. Detailed electron diffraction measurements on ternary TiNiCu films show strong evidence of epitaxially coupled Ti_2Cu precipitates that are only present in Ti-rich specimens.[22]

In order to investigate the cooling potential of the materials, temperature changes during mechanical cycling are studied by IR thermography in a number of tensile tests at different strain rates. These temperature changes occur within the materials during stress-induced martensite and reverse transformation. For detailed information, the reader may refer to Ref. 25. Under adiabatic conditions, which are reached at a strain rate of 0.2 s^{-1}, the peak changes of temperatures due to self-heating and cooling of the trained TiNi sample are ΔT_{load} = 16 K and ΔT_{unload} = −15 K, respectively. It has been shown in a previous work that the latent heat of sputtered TiNi film samples decreases due to functional fatigue upon mechanical cycling.[26] The corresponding temperature changes of the TiNiCuCo sample are +9 K and −12 K.

Subsequently, the design, fabrication, and performance of first demonstrator devices for actual heat pumping is evaluated.[23] The operation principle is shown in Fig. 2(a). Film samples of 20 mm length are attached to an alumina frame at both ends to create freestanding bridges (Fig. 2(b)). These bridges are mounted to a testing frame with linear guidance and placed in between a heat source and sink made from copper. The surface of the heat source is flat, whereas the heat sink has a convex surface. During operation of the demonstrator, the SMA film bridge is periodically moved between the source and the sink surface. When pressed to the convex sink (I.), the film is deflected out of plane and undergoes stress-induced phase transformation. Latent heat is released and transferred to the sink by conduction (II.). In the next half-cycle, the bridge is transferred to the flat heat source (III.). It cools down due to the endothermic reverse transformation and absorbs heat from the source (IV.).

The TiNi demonstrators comprise a heat source and sink assembled from individual copper segments.[23] The heat capacities of sink and source are 290 and 150 mJ/K, respectively. Width and thickness of the TiNi bridge are 1.75 mm and 20 μm, respectively.

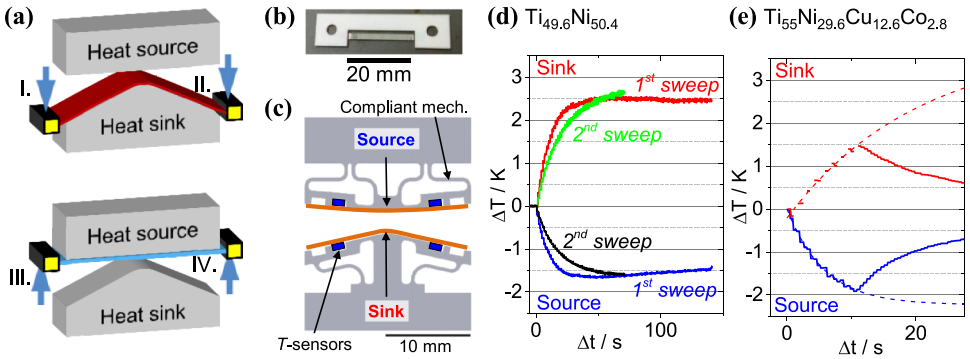

FIG. 2. (a) Schematic cooling cycle of SMA bridge-based elastocaloric cooling demonstrator: I. bridge is pressed against convex heat sink, II. latent heat is released to sink, III. bridge is moved to flat heat source, IV. latent heat is absorbed from source. (b) SMA foil bridge attached to alumina substrate. (c) Demonstrator device, comprising polymer frame with compliant mechanism, heat source and sink made from copper, including Pt100 temperature sensors. (d) Temperature evolution of sink and source of as-deposited TiNi device operated for 100 cycles at 0.72 Hz (first sweep). The curves of a second experimental sweep with the device after mechanical pre-cycling are included. (e) Temperature evolution of sink and source of TiNiCuCo device operated for 10 cycles at 0.75 Hz. Temperature forecasts based on exponential fits are included as dashed lines.

The transformation strain of the TiNiCuCo film is smaller than for the TiNi film. Also, the brittleness of the quaternary alloy is increased. Therefore, a modified demonstrator with a lower inclination angle of the heat sink surface is designed as depicted in Fig. 2(c). Sink and source consist of a single piece of bended copper sheet in order to omit sharp edges of copper segments. In both cases, the heat capacity is 50 mJ/K. The copper sheets are attached to a polymer frame with compliant mechanism, produced by stereolithographic 3D printing, in order to assure proper alignment of sink/source and SMA film during mechanical contact. Due to the lower critical stress of the quaternary alloy, samples with a higher cross section are used in this case, having a width and thickness of 3 mm and 39 μm, respectively.

The devices are operated by a spindle drive motor with a maximum velocity of 30 mm/s. Temperature changes of sink and source are monitored by IR thermography, as well as Pt100 temperature sensors attached to sink and source. The results are shown in Figs. 2(d) and 2(e). The displacement of the device as well as the applied forces is acquired. In the case of the TiNi demonstrator, two consecutive sweeps of the experiment are performed. During the first, a bridge device is operated for 100 cycles at 0.72 Hz. After about 20 cycles, the sink is heated up by 2.5 K and the source is cooled by −1.7 K. The cooling power is estimated to be 23.1 mW using the initial rate of temperature change of the source and its heat capacity. The work input dissipated by the device is determined to be 8 mW by numerical integration of the force-distance characteristic multiplied by the operation frequency. After 25 cycles, efficient heat transfer is not possible anymore, because the film device accumulates remanent strain, leading to buckling, while the thermal contact to the heat source degrades.

In order to investigate the cooling potential of a trained TiNi film, further cycles are investigated. Thereby, the displacement amplitude of the device is increased to guarantee full contact between TiNi bridge and heat source. The temperature changes of the second sweep are included in Fig. 2(d). Due to functional fatigue, a lower cooling power of 15.4 mW is achieved. However, the work input also decreases to 5 mW, because the stress-strain characteristic becomes narrower (compare Fig. 1(a)).

The TiNiCuCo bridge device is operated for 10 cycles at 0.75 Hz until the film broke due to brittleness. This performance is significantly improved by surface treatments like electro polishing,[22] which has not been performed in the present case. Since the ratio of thermal masses between sink/source and active material is lower in this case, the initial rates of temperature change are higher compared to the TiNi device. The temperature changes of sink and source reach +1.5/−2.0 K within 13 s (10 cycles). The estimated cooling power is 14.4 mW, whereas the work input is 5 mW. Interestingly, the cooling effect is stronger than the heating effect, although sink and source have

TABLE I. Performance characteristics of elastocaloric microcooling demonstrators. Legend: f–operation frequency, Δx–amplitude, ΔT_{cool}–temperature change of heat source, W_{cool}–cooling power, W_{mech}–work input of SMA material, COP_{cool}–coefficient of performance (input work of driving actuator is not considered).

Device	f/Hz	Δx/mm	Cycles	ΔT_{cool}/K	W_{cool}/mW	W_{mech}/mW	$COP_{cool} = W_{cool}/W_{mech}$
TiNi (as deposited)	0.72	5.9	100	−1.7	23.1	8	2.9
TiNi (pre-cycled)	0.69	6.5	48	−1.6	15.4	5	3.1
TiNiCuCo	0.75	4.4	10	−2.0	14.4	5	2.9

been designed with the same thermal mass. This observation has already been made in tensile or compressive tests on TiNiCuCo,[25] FePd,[27] and NiMnSn[28] samples, which is unexpected, because irreversible processes like internal friction should contribute to heating and mitigate cooling. An explanation is still to be found and might be related to differences in the enthalpy of forward and reverse martensitic transformation, or changes in specific heat capacity during stress-induced transformation. However, a temperature forecast for the sink and source temperature, based on exponential fits, predicts a heating effect eventually exceeding the cooling effect after a sufficient number of cycles (Fig. 2(e)).

The performance characteristics of the demonstrators are summarized in Table I. The coefficient of performance COP is given by the ratio of transferred heat and work input per cycle. The work input is estimated from the force-distance characteristic, i.e., the COP value given here does not take into account the input work used for driving the actuator. The COPs of the untrained TiNi device as well as trained TiNi and TiNiCuCo devices are 2.9, 3.1, and 2.9, respectively. The above investigations show that elastocaloric micro-cooling can be performed with high efficiency based on sputter deposited TiNi and TiNiCuCo films. In the case of TiNi, strong functional fatigue effects are observed within the first tens of cycles, leading to a decrease in elastocaloric effect size. However, the mechanical work input decreases likewise, so that a cooling device operated with a TiNi film after mechanical pre-cycling reaches even a slightly higher COP, compared to the as-deposited film. However, a remanent strain in the order of 1% is accumulated. This leads to a strong buckling effect, which has to be compensated by device design making the TiNi film unattractive for long-term operation. Quaternary TiNiCuCo films show a slightly weaker elastocaloric effect. On the other hand, the work input is also considerably lower and transformation forces are lower than for TiNi. Moreover, TiNiCuCo microcooling devices reach the same COP as TiNi devices but do not accumulate remanent strain. Therefore, they are predestined for high-efficiency microcooling applications.

The authors gratefully acknowledge funding by the German Science Foundation (DFG) within the priority program No. SPP1599 “Caloric Effects in Ferroic Materials: New Concepts for Cooling” (www.ferroiccooling.de) and funding of the Bruker D8 through the Helmholtz Energy Materials Characterization Platform (HEMCP) initiated by the Helmholtz Association and coordinated by Forschungszentrum Jülich.

[1] S. Fähler, U. K. Rößler, O. Kastner, J. Eckert, G. Eggeler, H. Emmerich, P. Entel, S. Müller, E. Quandt, and K. Albe, Adv. Eng. Mater. **14**, 10 (2012).
[2] L. Mañosa, A. Planes, and M. Acet, J. Mater. Chem. A **1**, 4925 (2013).
[3] X. Moya, S. Kar-Narayan, and N. D. Mathur, Nat. Mater. **13**, 439 (2014).
[4] I. Takeuchi and K. Sandeman, Phys. Today **68**(12), 48 (2015).
[5] X. Moya, E. Defay, V. Heine, and N. D. Mathur, Nat. Phys. **11**, 204 (2015).
[6] J. Cui, Y. Wu, J. Muehlbauer, Y. Hwang, R. Radermacher, S. Fackler, M. Wuttig, and I. Takeuchi, Appl. Phys. Lett. **101**, 073904 (2012).
[7] W. Goetzler, R. Zogg, J. Young, and C. Johnson, *Energy Savings Potential and RD&D Opportunities for Non-Vapor-Compression HVAC Technologies* (Navigant Consulting, Inc., U.S. Department of Energy, Burlington, MA, 2014).
[8] L. Mañosa, A. Planes, E. Vives, E. Bonnot, and R. Romero, Funct. Mater. Lett. **2**, 73 (2009).
[9] J. Otubo, O. D. Rigo, A. A. Coelho, C. M. Neto, and P. R. Mei, Mater. Sci. Eng. **481-482**, 639 (2008).
[10] J. Frenzel, A. Wieczorek, I. Opahle, B. Maaß, R. Drautz, and G. Eggeler, Acta Mater. **90**, 213 (2015).
[11] E. A. Pieczyska, H. Tobushi, and K. Kulasinski, Smart Mater. Struct. **22**, 035007 (2013).
[12] S. Qian, J. Ling, J. Muehlbauer, Y. Hwang, and R. Radermacher, Int. J. Refrig. **55**, 102 (2015).
[13] S. Qian, J. Ling, Y. Hwang, R. Radermacher, and I. Takeuchi, Int. J. Refrig. **56**, 65 (2015).

[14] S. Qian, A. Alabdulkarem, J. Ling, J. Muehlbauer, Y. Hwang, R. Radermacher, and I. Takeuchi, Int. J. Refrig. **57**, 62 (2015).
[15] J. Tušek, K. Engelbrecht, R. Millán-Solsona, L. Manñosa, E. Vives, L. P. Mikkelsen, and N. Pryds, Adv. Energy Mater. **5**, 1500361 (2015).
[16] M. Schmidt, J. Ullrich, A. Wieczorek, J. Frenzel, A. Schütze, G. Eggeler, and S. Seelecke, Shape Mem. Superelasticity **1**, 132 (2015).
[17] S. Qian, Y. Wu, J. Ling, J. Muehlbauer, Y. Hwang, I. Takeuchi, and R. Radermacher, "Design, development and testing of a compressive thermoelastic cooling prototype," in 24th International Congress of Refrigeration (ICR2015), Yokohama, Japan (submitted).
[18] M. Schmidt, A. Schütze, and S. Seelecke, Int. J. Refrig. **54**, 88 (2015).
[19] A. Majumdar, Nat. Nanotechnol. **4**, 214 (2009).
[20] J. P. Carmo, M. F. Silva, J. F. Ribeiro, R. F. Wolffenbuttel, P. Alpuim, J. G. Rocha, L. M. Goncalves, and J. H. Correira, Microsyst. Technol. **17**, 1283 (2011).
[21] H. Ossmer, F. Lambrecht, M. Gültig, C. Chluba, E. Quandt, and M. Kohl, Acta Mater. **81**, 9 (2014).
[22] C. Chluba, W. Ge, R. Lima de Miranda, J. Strobel, L. Kienle, E. Quandt, and M. Wuttig, Science **348**, 1004 (2015).
[23] H. Ossmer, S. Miyazaki, and M. Kohl, in *Proceedings of the Transducers 2015*, *Anchorage, USA* (IEEE, 2015), p. 726.
[24] R. Lima de Miranda, C. Zamponi, and E. Quandt, Adv. Eng. Mater. **15**, 66 (2013).
[25] H. Ossmer, C. Chluba, M. Gueltig, E. Quandt, and M. Kohl, Shape Mem. Superelasticity **1**, 142 (2015).
[26] C. Bechtold, C. Chluba, R. Lima de Miranda, and E. Quandt, Appl. Phys. Lett. **101**, 091903 (2012).
[27] F. Xiao, T. Fukuda, and T. Kakeshita, Appl. Phys. Lett. **102**, 161914 (2013).
[28] W. Sun, J. Liu, B. Lu, Y. Li, and A. Yan, Scr. Mater. **114**, 1 (2016).